

Variation of the Solar Mg II Spectral Lines Across the Solar Disk and the Solar Cycle

—¹

¹ University of Glasgow, Kelvin Building, University of Glasgow, Glasgow, Scotland

ABSTRACT

The Mg II h&k emission lines provide a wide range of diagnostic capabilities for study of the solar chromosphere, however until the launch of Interface Region Imaging Spectrograph (IRIS) in-depth study of these lines has been limited. This work uses a double-Gaussian model to fit Mg II h&k profiles taken from full-sun mosaics. Using many of these profiles a study of the variation of the line profile across the solar disk in the network and internetwork was performed, before using these variations to infer the variation of the solar atmospheric properties. It is seen that in both Mg II h and Mg II k that across the disk the median intensity in the peaks and the central core depression increases from the solar limb to $\mu = 0.9$ before decreasing again towards the disk centre. This observed variation in the intensity of the central depression implies that the height of the transition region decreases moving in from the solar limb to $\mu = 0.9$ before being found at increasing heights from there to the disk centre. The observed variation in the peak intensity implies that the plasma temperature increases from the limb to the same point on the disk before again dropping slightly approaching the disk centre. Seen throughout the disk is the predisposition for the violent side peak in the profiles to be the stronger of the two peaks with no apparent dependency on disk location, this implies that the velocity within the atmosphere also lacks any such dependence. The final step of the investigation was to consider how the solar cycle affected the emission profiles, this study yielded evidence that the observed intensity of the emission lines is correlated with the solar activity, and that there is a possible link between shorter term variations in solar activity and similar short term variations in the emission line profiles.

1. INTRODUCTION

The study of the chromosphere is an ongoing active area of research within solar physics. As with so much of solar observation much of this work is done through the study of spectral lines. For many years one of the strongest spectral lines has been hidden from us; our atmosphere shielding us from UV radiation and consequently blinding us the Mg II h&k lines found at 2803.5 Å and 2796.6 Å respectively. Due to the difficulty in observing these spectral lines it was not until the advent of rocketry that it was possible to make measurements using instruments mounted to rockets (Durand et al. 1949).

The seminal work in the study of the variation of the Mg II h&k lines over the solar disk was carried out using a telescope-spectrograph mounted to a rocket (Kohl & Parkinson 1976) which due to the short duration of observation was only able to make observation of the lines at two quiet sun locations; this nevertheless demonstrated clearly that a variation in the emission line is present across the solar disk.

More recently the launch of the Interface Region Imaging Spectrograph (IRIS) (De Pontieu et al. 2014) has

provided unprecedented resolution for observations of the Mg II lines, allowing for improved studies of these emission lines, comparison with modelled solar atmospheres and improved plasma diagnostics. Using IRIS Schmit et al. (2015) have been able to study the variation if the Mg II h line from the disk centre to limb. As they were able to isolate many thousands of spectra across the solar disk they were able, after assigning a model to the line profile, to develop in-depth descriptions of the spatial variation of various elements of the line profile. In addition to this they were able to identify differences in the variations in different solar regions.

Similar work, however, has not been carried out to study the centre-to-limb variation of the Mg II k line which is formed at a slightly different height in the solar atmosphere providing additional, complimentary information about the chromospheric plasma. In addition to this it is as yet unknown how, if at all, the solar cycle affects the emissions profiles and their centre-to-limb variation.

1.1. *Mg II Line Formation*

The formation of the Mg II lines is a complex problem as they are formed in the chromosphere, which is opti-

cally thick of the Mg II h&k lines meaning that the assumption of Local Thermodynamic Equilibrium (LTE), usually employed in Solar Physics does not apply. Additionally the Mg II lines are subject to Partial Frequency Redistribution (PRD) (Milkey & Mihalas 1974) the effects of which are difficult to model in a non-LTE environment; consequently modelling these emission lines is an involved problem that has not yet been wholly solved. Currently the most accurate model was developed by Leenaarts et al. (2013a) using a four-level plus continuum atom to model the emission properties of Mg; their work however does not provide a complete model as that requires a full 3D treatment of radiative transfer as the models in use at the time of this investigation did not accurately solve for PRD effects when the assumption of LTE is removed, although more recent models now allow for this (Kerr et al. 2019). The compromise employed by the model to overcome this issues is to use a 1D description of radiative transfer that does accurately include PRD effects to model the line profile through the wings and to the peaks and to use a 3D description that assumes complete redistribution for the central depression.

1.2. *Mg II Plasma Diagnostics*

Using the previously developed model Leenaarts et al. (2013b) demonstrated the applicability and versatility of Mg II lines as diagnostic tools for chromospheric plasma properties, identifying a vast array of correlations and anti-correlations.

They found that the Doppler shift of the central depression for both the Mg II h&k is strongly correlated (correlation coefficient ~ 1) to the vertical velocity at optical depth unity, which is found below the Transition Region. As the heights where optical depth of unity occurs at slightly differing heights for each of the lines it is possible to take these Doppler shifts in combination to reconstruct the sign, and with suitably accurate measurement, the magnitude of the velocity gradient immediately below the Transition Region. In addition to these correlations, the intensity of the central depressions has been identified as being weakly anti-correlated with the height of formation i.e. the height where the optical depth ~ 1 . Thus it is possible to use this to map across the surface of the sun the height of the Transition Region.

The peaks of the emission profiles reveal different properties of the plasma; the intensities of the emission peaks have been found to be correlated to the temperature and the height of formation, with this correlation being strongest for the most intense emission lines. As the Mg II lines each feature two distinct peaks which

form a slightly different heights, deeper than the central depression, the observed difference in wavelength between these peaks is correlated to the velocity gradient in the upper chromosphere. Furthermore, the ratio of the intensities of each of the peaks is strongly correlated to the average velocity seen in the upper chromosphere.

1.3. *The Quiet Sun*

Often discussed are active regions of the sun, such as sunspots or CMEs the low activity counterpart to this is the Quiet Sun. In studies of the emission lines it is often useful to consider the Quiet Sun; as due to its relatively lower activity there are less factors contributing to complicating observations. The definition of the Quiet Sun is not clearly delineated and its definition can vary from study to study as needed however it can be taken in general terms to be regions of the sun with an unsigned line-of-sight magnetic field strength below 200G (Sánchez Almeida & Martínez González 2011).

The Quiet Sun can be further subdivided into two different regions based upon the magnetic and flux emitting profiles namely the network and the internetwork, the origins of which are currently not well understood.

The network is observed to surround the borders of the supergranular cells, whereas the the internetwork is found within said cells. The network is observed to be the magnetically dominant of the two features with magnetic fields occasionally exceeding the normal quiet sun limit reaching strengths of 10^3 G compared to the internetwork which shows field strengths on the order 10^2 G or less (Solanki 1993). Due to this and the internetwork being found within the network it can only be detected using high resolution magnetograms. These show the internetwork as small isolated features which move towards the network during their lifetime, which is on the order of less than 10 minutes. The network and internetwork are inextricably linked and it is currently understood that the internetwork is the primary source of flux in the network and that consequently the internetwork is the most important contributor of flux to the Quiet Sun, with some observations suggesting that half the Quiet Sun flux could be contained within the internetwork (Gošić et al. 2014).

1.4. *The Solar Cycle*

The activity levels of the sun are not constant. The variation in solar activity was first identified in 1775 by Christian Horrebow who noted the periodicity in the number of sunspots observed on the sun over a number of years (Jørgensen et al. 2019). This periodicity was formalised and recognised as an 11 year cycle later by Schwabe (1843); each of these 11 year cycles are measured to run from one solar minima (the time of lowest

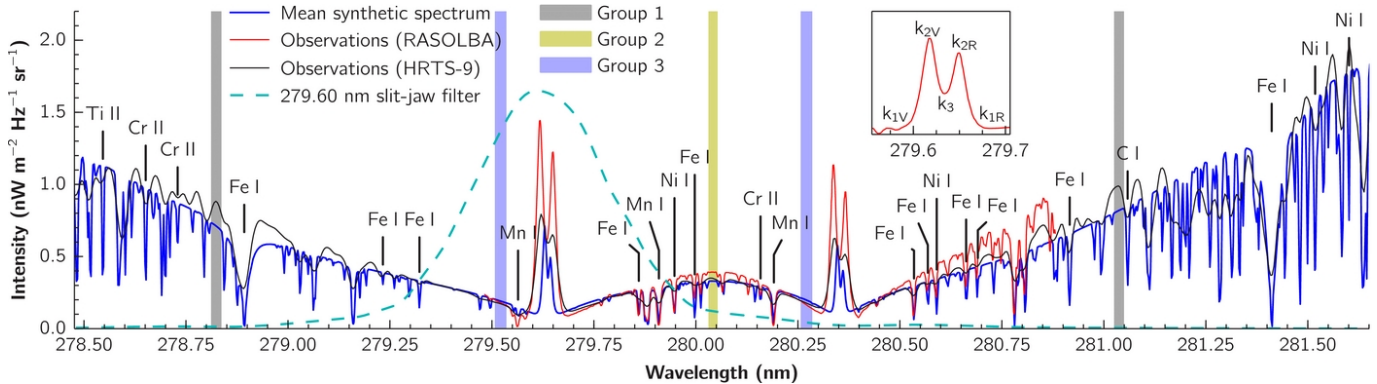


Figure 1. Extract of the solar spectrum from Pereira et al. (2013) showing a synthetic spectrum and observations from RASOLBA and HRTS-9. The spectrum includes the Mg II lines of interest at 279.6nm and 280.3nm

solar activity and fewest sunspots) to the next. In addition to the raw variation of solar activity Carrington (1858) and Spörer (1880) identified Spörer Law describing how the latitude of sunspot formation varies across the solar cycle.

Having discovered the magnetic nature of the sun, and sunspots (Hale 1908) a periodicity linking this to the solar cycle was subsequently identified. It was discovered that the polarity of the magnetic field was dependent upon which side of the equator was under observation, and that whilst the polarity was constant across a solar cycle it alternated across the equator with it (Hale et al. 1919).

This temporal variation inherent to the activity levels of the sun means that any attempt to understand the behaviour that the sun is presenting is not only based on a snapshot from those observations studied but is also a snapshot of the sun at any given point in the solar cycle. Therefore to gain a full appreciation of solar behaviours it is necessary to consider how these effects affect different processes.

This work seeks to study the spatial variation of the Mg II h&k lines in quiet sun, differentiating between the network and the internetwork, and then attempting to investigate how these spatial variations themselves vary across the solar cycle. §2 describes the data used throughout the study; §3 discusses how this data was subsequently processed into the results presented in §4.

2. DATA

IRIS data is provided with several different levels of preprocessing applied to it, in this paper level 2 data is used. This removes bad pixels from dust on the detector, performs the necessary dark current and flat field corrections, and performs geometric and wavelength cal-

ibrations based on the rest wavelength of Ni I 2799.17Å (Pereira et al. 2019).

Observations of the sun by IRIS are made in three separate UV windows 1332-1358Å, 1381-1407Å, and 2783-2834Å. Spectral information is obtained by passing incident solar light onto a grating, the spatial width of which is limited by the 175Å width of the slit. IRIS normally observes only a subsample of the solar disk, however once per month it is instructed to generate a full disk mosaic.

Full disk mosaics are produced by combining a series of 184 observations of the solar disk, taken over as short a time period as is possible. Each of the individual observations is made up of a 64 step raster in 2 arcsecond steps with 2 second exposure time at each slit position. The spectra along the slit are binned to 0.66 arcseconds which gives an observed area of 128 x 175 arcseconds for each observation. With each observation taking approximately 190 seconds it takes \sim 18 hours to build up the entire set including the time taken to repoint the satellite.

For the study of the Mg II emission lines it is not necessary to make analyses of all the data taken by IRIS, instead analysis is limited to spectral windows 3.4 Å wide centred upon 2803.5 Å and 2796.6 Å encompassing each of the spectral lines of interest.

In order to identify Quiet Sun regions within the IRIS mosaics these are compared with observations from the Helioseismic and Magnetic Imager (HMI) ([Scherrer et al. 2012](#)) aboard the Solar Dynamics observatory. HMI is capable of providing whole disk measurements of the line of sight component of the solar magnetic field with a cadence of 720 seconds. In order to make these as directly comparable as possible to the IRIS mosaics several of these observations are combined to create a pseudo-mosaic, whole disk line of sight magnetic field

map, which matches the time of the IRIS observations as closely as possible. For each mosaic produced by IRIS such an accompanying pseudo-mosaic is provided. Shown in figure 2 is such an IRIS mosaic and corresponding HMI pseudo-mosaic.

The Mg II emission lines take on a complex double peaked form with rising wings upon their either side. Shown in figure 1 is the solar emission spectrum in the region of the Mg II h&k lines. The complexity of these lines should be immediately apparent with both showing an asymmetric double peak with rising wings which also contain spectral features.

3. METHOD

In order to model the Mg II h&k emission lines a nine parameter double-Gaussian fit was employed to fit the aforementioned spectral windows (Schmit et al. 2015):

$$I(\lambda) = a + b * |\lambda - c| + d * \left(\exp\left(\frac{-(\lambda-f)^2}{g^2}\right) - h * \exp\left(\frac{-(\lambda-j)^2}{k^2}\right) \right) \quad (1)$$

This model makes no attempt to incorporate the physics of the solar atmosphere, and thus is incapable of determining the source function or a true theoretical profile. However it is capable of producing single and double peaked Gaussians which closely represent the emission profiles of the Mg II h&k. The profile represented in equation 1 is constructed from a wide positive Gaussian (the first exponential term) superimposed with a narrow negative Gaussian (the second exponential term). The leading linear terms encapsulates the wings of the profile. This process is applicable to both Mg II h&k lines, however analysis of Mg II k is complicated by an Mn I line at 2795.6Å.

In order to fit the model to the data the MPFIT least squares minimisation algorithm (Markwardt 2009) was used to identify the best fit model by χ^2 . In fitting the model it was assumed that the errors were Poissonian in nature. Following the procedure to model the emission profiles the number and location of the various extrema found in each profile was determined. Most of the profiles take on a double peaked appearance having two maxima - one toward the red and another the violet side of the spectral window known as $h2r$ or $k2r$, and $h2v$ or $k2v$ respectively. The wings of profiles also tend to maxima approaching each far side of the spectral window. These taken together lead to three local minima, $h1r$ or $k1r$, and $h1v$ or $k1v$ found at the minima of the wings before the peaks, and $h3$ or $k3$ the central depression between the peaks. Having identified these features their fitted intensity was recorded for each best fit mod-

elled profile. In addition to the double peaked profile, those which only contained a single peak are also possible and the intensity of the single peak was accordingly recorded.

In using χ^2 as a metric to determine the quality of fit it was possible to identify those fitted models that had been possible to fit but were poor representations of the data. This was done by setting a χ^2 threshold above which a model would be considered insufficiently accurate. The threshold for model acceptance was set at $\chi^2 < 1.5$, with this threshold approximately 80% of profiles, varying by 2-3% by mosaic, could be fitted accurately.

Figure 3 (a) and (b) show typical profiles in the quiet sun for Mg II h observed by IRIS and their associated fits, (a) has a χ^2 value of 1.004, whilst (b) has a χ^2 value of 0.911. This, in combination with the high percentage acceptance, suggests that this model is accurate and suitable for modelling the Mg II h line. Furthermore the low χ^2 value seen across all the fitted profiles suggests that the errors which have been associated with the data points are a pessimistic estimation of the quality of the data.

Figure 4 (a) shows the profile for a Mg II k line in a quiet sun region, it is immediately apparent that it is similar in form to the Mg II h line exception for the additional peak seen to the violet side, this can be attributed to the aforementioned Mn I line. In order to successfully fit profiles to the Mg II k line it is necessary to carefully constrain the spectral window under observation. Shown in figure 4 (b) is the same profile as in (a) under a constrained window, this fit using the model in equation 1 shows a χ^2 value of 0.438 demonstrating the validity of constraining the spectral window.

In addition to study of the intensity of the maxima and minima, in order to get a fuller appreciation of the profiles and their variation, as well as allowing for study of the plasma diagnostics two additional parameters are calculated; asymmetry and relative depth.

$$A_* = \frac{I_{*2v} - I_{*2r}}{I_{*2v} + I_{*2r}} \quad (2)$$

$$D_* = 1 - \frac{2I_{*3}}{I_{*2v} + I_{*2r}} \quad (3)$$

In each of these equations * denotes either the h or k line, whichever is under study. The asymmetry statistic describes the relative difference between the height of the two peaks spanning from 1 to -1, where a positive value describes a profile where the violet side peak is the more intense and conversely a negative value is associated with a profile where the red side peak is the

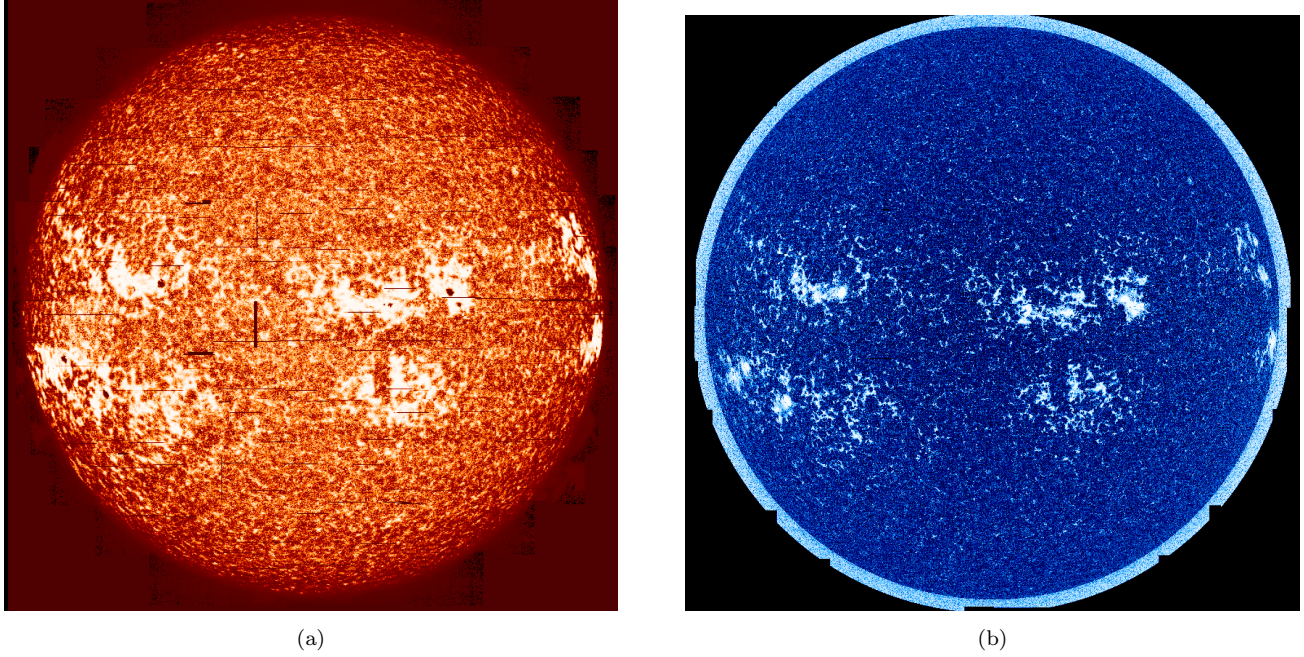


Figure 2. (a) IRIS Full Disk Mosaic from 24th August 2014, intensity summed across Mg II h spectral window. (b) Corresponding HMI pseudo-mosaic.

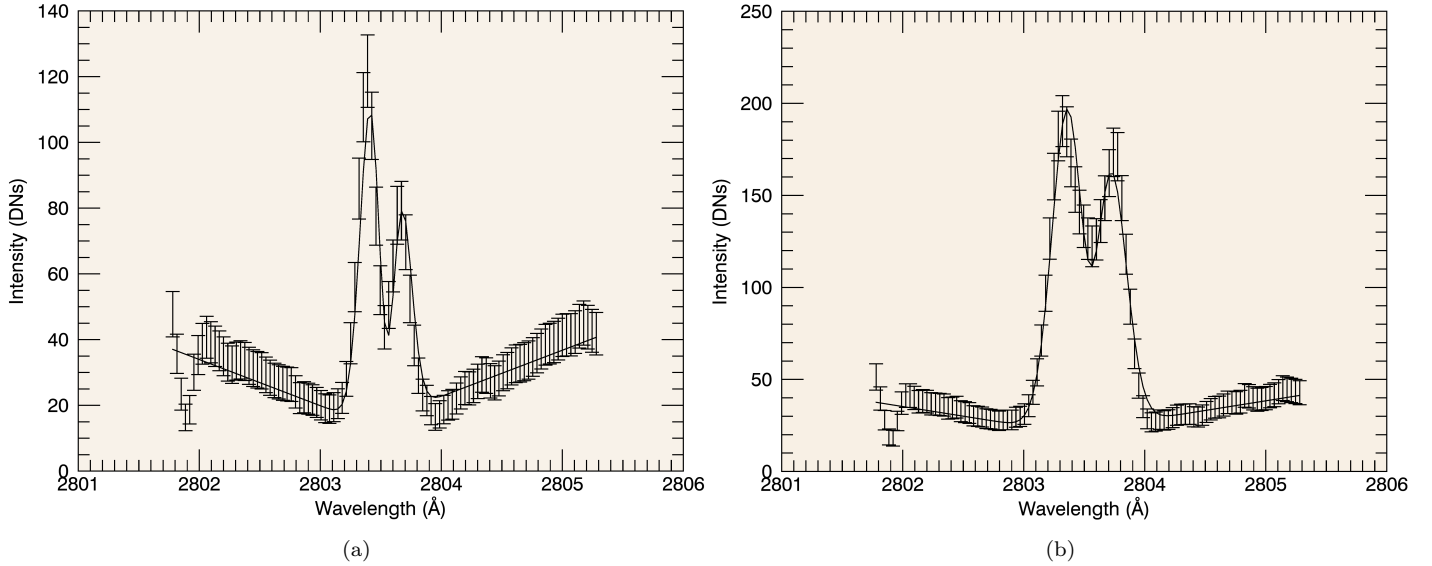


Figure 3. Typical double peaked profiles taken from quiet sun regions for MgII h with differing χ^2 values; (a) 1.004 and (b) 0.911. The error bars show the IRIS data. The solid line shows the best fit model.

dominant. An asymmetry value of 0 is associated with the case where both peaks are of equal intensity.

The relative depth is a measure of the depth of the central core depression and spans between 0 and 1. A depth statistic of 1 relates to the case where both peaks are fully localised as separate profiles with the depression reaching to as low as to be indistinguishable from

the continuum. By contrast a value of 0 describes a profile that has no core depression.

To study spatial variation of the emission profiles and the properties of the features of interest were plotted against the value μ , (the cosine of the heliocentric angle, the angle between the line of sight and normal), corresponding to the location of the profile where $\mu = 1$

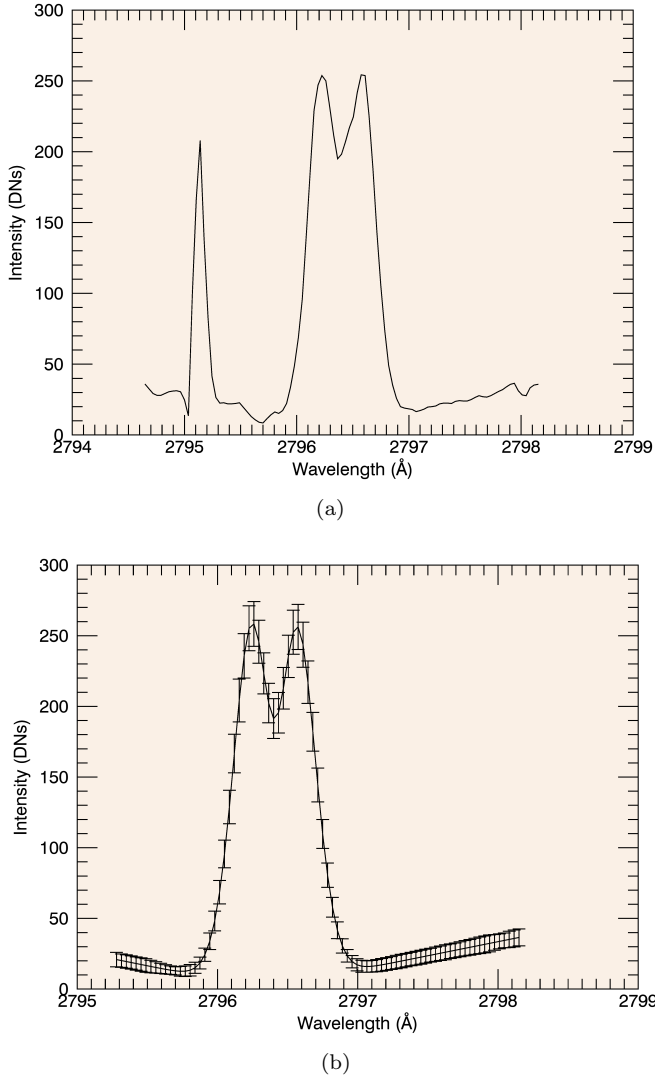


Figure 4. (a) A typical profile taken from a quiet sun regions in MgII k. (b) The same profile in a constrained spectral window. The error bars show the IRIS data. The solid line shows the best fit model.

corresponds to the disk centre and $\mu = 0$ is found at the solar limb.

In order to study the temporal variations in the emission profiles the median value for the features of interest were extracted for several values of μ from each of the mosaics under investigation; these were then used to generate an appropriate set of time series plots.

Throughout the study effort was made to distinguish between profiles that were associated with the network and profiles that were associated with the internetwork. Combining the definition for quiet sun from Sánchez Almeida & Martínez González (2011) and the work previously performed by Schmit et al. (2015) internetwork was defined as pixels seen in HMI to have unsigned line-

of-sight magnetic field strength below 60G and that only 5% of said pixel's neighbours within a radius of 5 pixels could exceed this threshold. The network was defined to be pixels which showed an unsigned line-of-sight magnetic field strength of 60-200G. In order to be accepted as a network pixel 15% of the pixels within a 5 pixel radius of the pixel of interest must also meet the same conditions.

In order to accurately identify the Quiet Sun pixels in the IRIS data from those identified in HMI it was necessary to make the data sets directly comparable, which necessitated reshaping both the IRIS mosaics and the HMI pseudo-mosaics. IRIS Mosaics were provided with an x-y shape of 6011 by 1001 pixels whilst the HMI pseudo-mosaics were provided at 4096 by 4096. In order to avoid introducing “new data” by using interpolation to expand the dimensions the resolution was instead degraded by reshaping each to 4096 by 1001 – the smaller of each dimension. Although this results in discarding data it avoids introducing spurious data which could adversely affect the reliability of the results.

4. RESULTS

In order to clearly present the spatial variation of the emission profiles it was necessary to bin the values of μ , therefore in the results that follow for the spatial variation the results are presented at 0.01 increments of μ . In the case of time series analysis each of the values of μ that are taken are extracted from this same binning procedure so as to ensure direct comparability across the presented results.

Boxplots are used to concisely present the results in fashion that is easy to understand; due to the high number of profiles studied a plot containing every data point would be so dense as to be ambiguous. The boxplot in contrast condenses the results to show both the full extent of the data points and indicate the values they most densely cluster around.

4.1. Centre-to-Limb Spatial Variation of Mg II h

Initial study of the centre-to-limb variation is performed using a mosaic constructed from observations taken on August 24th 2014, which allows for comparison performed by Schmit et al. (2015). Shown in figures 5 and 6 is the variation across the solar disk in the network and internetwork of $h2v$, $h2r$, $h3$ and the asymmetry and depth statistics.

Studying these plots it is immediately apparent that there are many similarities and differences between the network and the internetwork. In all three features shown in figure 5 the intensity appears to grow from the limb towards the centre with a slight drop off in intensity above $\mu = 0.95$. Furthermore the spread of results

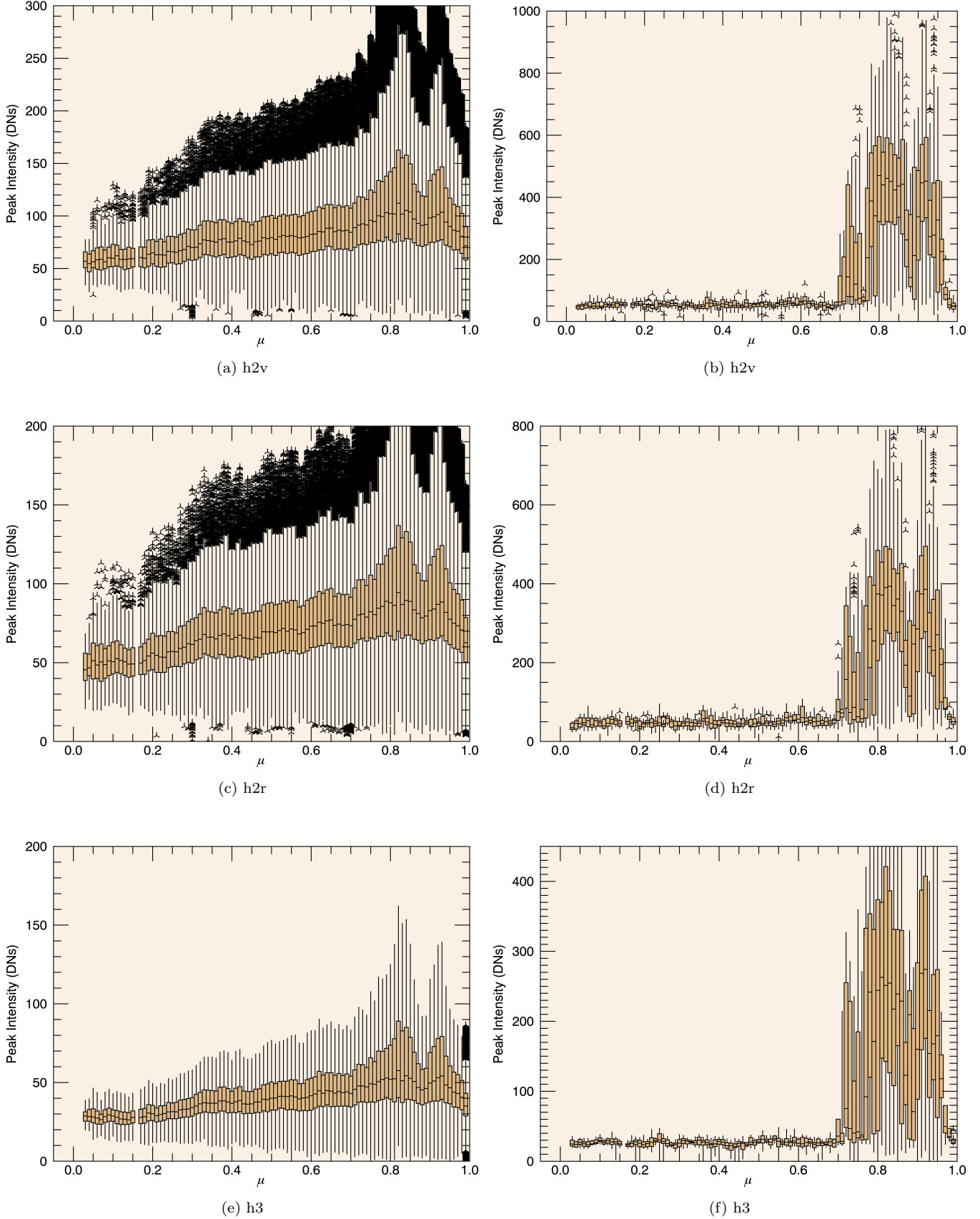


Figure 5. The centre-to-limb variation in (a) solar internetwork h2v and (b) solar network h2v, (c) solar internetwork h2r (d) solar network h2r, (e) solar internetwork h3 and, (f) solar network h3. The tri-cross represent suspected outliers in the fitted peaks, the boxes encompass the upper and lower quartiles, the line within the boxes denotes the median and the lines extending from the boxes indicate the maxima and minima extent.

demonstrates growth from the limb to centre, with both the spread of the upper and lower quartiles growing but also the range that the maximum and minimum values take. Once again this effect is marginally reversed above $\mu = 0.95$.

The most inherent difference between the network and internetwork is the order of magnitude of the observed intensity, this is an expected difference between the network and internetwork as the former is always seen as the brighter of the features. One of the most striking differences between the network and the internetwork is the sudden increases seen at $\mu = 0.7$ in the features in the network; this can be attributed, in part, to the number of profiles studied. In the network there were ~ 6900 profiles in comparison to $\sim 130,000$ in the internetwork. Taking this in combination with the more network profiles being found near the solar centre, and thus there being more opportunity for spread in intensity presents a possible explanation for sudden increase in intensity and spread of the intensity of the network features.

Figure 6 shows the centre-to-limb variation of the asymmetry and depth statistics in the internetwork and network as constructed from the observations in figure 5. In both the network and internetwork the profiles always tend to have a slightly more intense violet side peak, although with a minority of profiles showing a more dominant red side peak. The centre-to-limb variation seen in the network and internetwork show significant differences. In the network the asymmetry and its distribution remains approximately constant across the disk, with the upper and lower quartiles showing significant overlap from one bin to the next. The only significant variation seen in the network is at $\mu > 0.8$ where the distribution of the statistic becomes much narrower.

The variation of the asymmetry in the internetwork is markedly different from that of the network. Across the disk the internetwork asymmetry and its spread remains approximately constant, with an increasing number of suspected outliers moving towards the solar centre. The variation of the asymmetry in the network is much more erratic; quite possibly in part due to reduced number in profiles under investigation. Despite these differences both the network and the internetwork consistently show a majority of profiles have a positive asymmetry statistic meaning that across the solar disk the most predominant profile is one where the violet side maxima is the more intense.

Like the previous features and statistics discussed, the relative depth in the network and the internetwork show a range of similarities and differences. Both of them show that across the disk the dominant profile has a

central depression which separates the profile into the expected double peaked shape. Equally the majority, and indeed there are only a very small number of outliers to the contrary, do not have a central core depth that separates the maxima into two localised peaks. Similar to the behaviour seen in the asymmetry statistic the network contains a significantly more spread in values than the internetwork. Although present in the network, it is most obvious in the internetwork, that at $\mu = 0.95$ the depth of the central depression increases. This increase in depth coincides with the decrease in the observed intensities as previously discussed, indicating that the reduction in $h3$ intensity is relatively greater than that observed in the peaks.

The analysis of the spatial variations seen in the Mg II h line features and statistics show good agreement with the spatial variation identified by Schmit et al. (2015) in their analysis of the same data set.

4.2. Centre-to-Limb Spatial Variation of Mg II k

Figures 7 and 8 similarly show the spatial variation of the Mg II k line across the solar disk on August 24th 2014, which allows for comparison between the variation seen in the Mg II h emission profiles. As is expected the observed intensity of each of the features of interest is higher in Mg II k than in Mg II h, due to the former being the stronger emission line.

The spatial variation in the features seen in Mg II k are similar to those seen in Mg II h. Once again the intensity grows from the solar limb to the disk centre which is associated with the an increase in the spread of intensities observed with an inversion of this trend also seen at $\mu = 0.95$. As was also seen in the network in Mg II h there is a sudden increase in the observed intensity in the network at $\mu = 0.7$, as before this can in part be attributed to the number and location of the profiles identified as being in the network.

Despite the similarities in the variations seen in each of the lines there are some differences that can be seen. The gradients in the variations are greater in Mg II k, both when rising towards the centre and then falling at $\mu > 0.95$. In addition to this there is less of a spread seen in the observed intensities, in particular in the the range spanned by the lower and upper qualities is smaller in Mg II k than in Mg II h showing that the observed intensities tend to cluster around the same values more in Mg II k.

The behaviour of the asymmetry and depth statistics follows a similar pattern to those seen before. The variation in both of these statistics for the network is, once again, far more erratic in the network than in the internetwork; although as before this may be attributed to

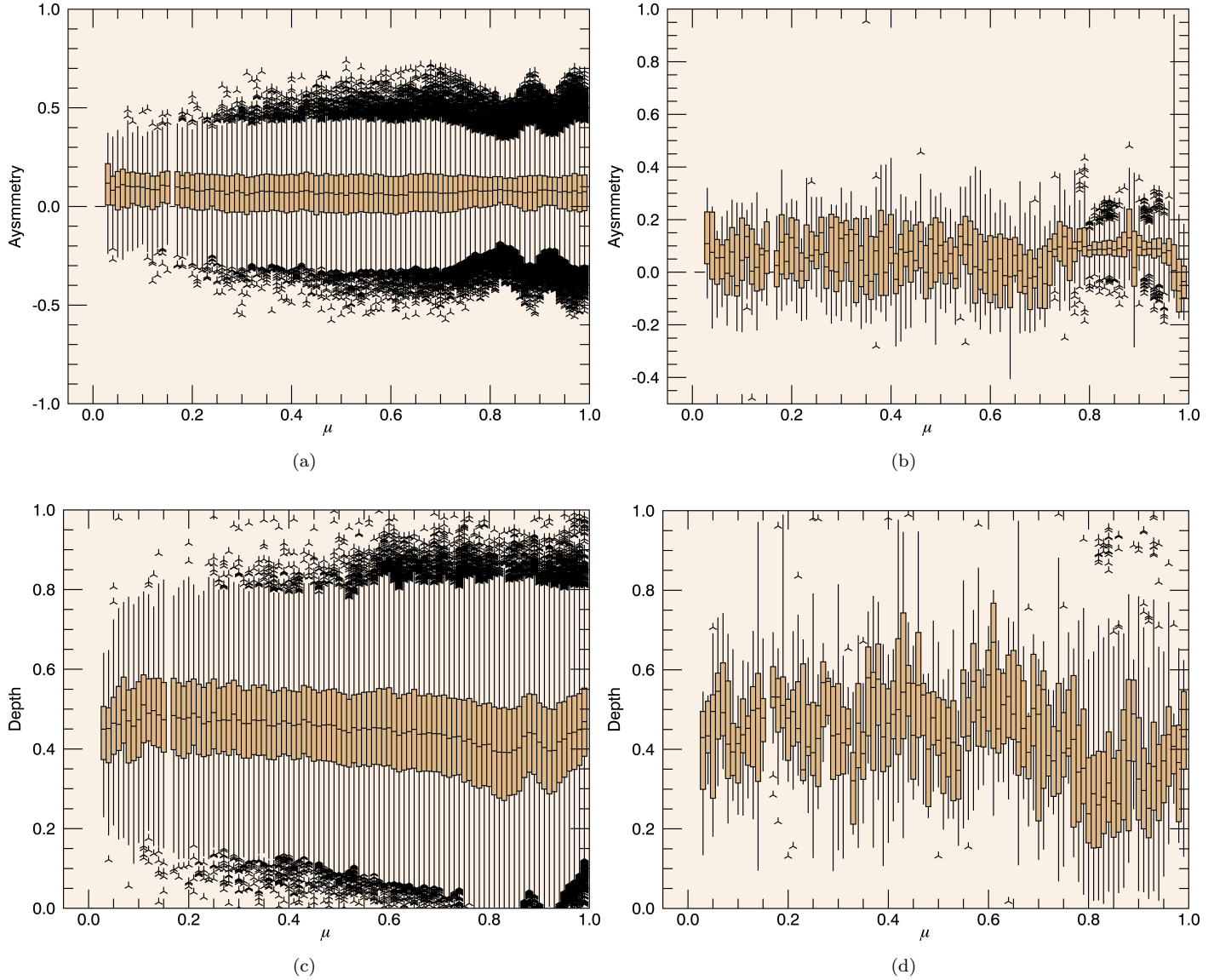


Figure 6. As figure 5. The centre-to-limb variation in (a) asymmetry in the solar internetwork, (b) asymmetry in the solar network, (c) central core relative depth in the solar internetwork, and (d) central core relative depth in the solar network.

there being significantly fewer network profiles. Regardless there are some noticeable differences between both the network and the internetwork, and Mg II k and Mg II h. The Mg II k network profiles show a far greater tendency to a positive asymmetry value than either the internetwork or the Mg II h network profiles; although both of these consistently and predominantly were found to have a positive value they all have a range of values which extend down to a negative value – in Mg II k however although this happens the incidence is far rarer and the negative values seen are of smaller magnitude.

Similar to that seen in figure 7 where the gradients of the feature variations are larger than in Mg II h the gradient of the increase of the relative depth at high μ in

Mg II k is also larger and more pronounced. This once again identifies that the intensity of h_3 decreases more than that of the maxima.

4.3. Centre-to-Limb Variations in Plasma Diagnostics

From §4.1 & 4.2 it is apparent that despite some differences in magnitudes there are many similarities in the spatial variation of each of the Mg II lines especially when comparing the variation of the line profile in the same Quiet Sun regions. When considering the plasma diagnostics this is to be expected as the plasma diagnostic relations identified and developed by Leenaarts et al. (2013b) are applicable to both Mg II h and Mg II k profiles. These similarities in the behaviours mean that at

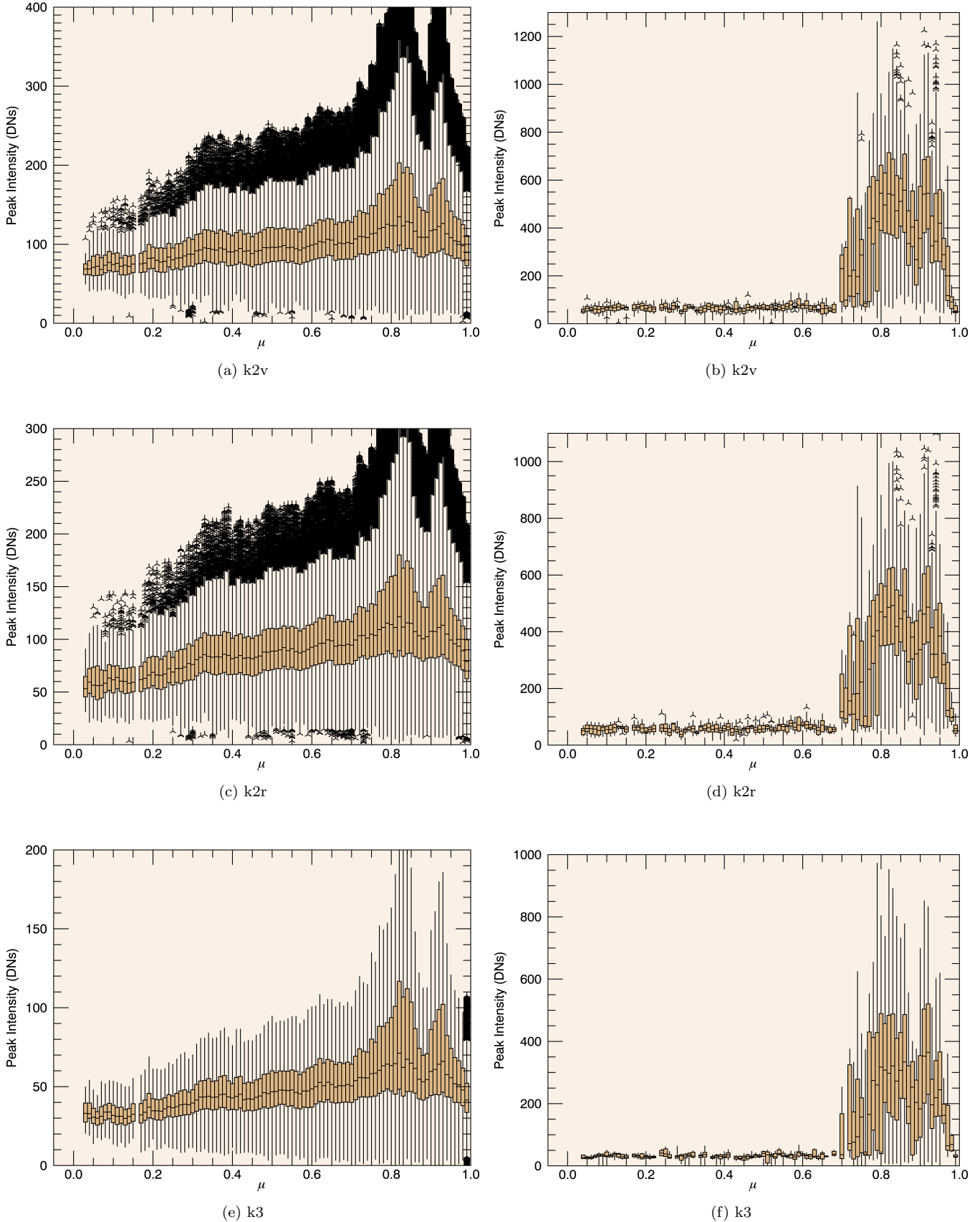


Figure 7. As figure 5. The centre-to-limb variation in (a) solar internetwork k2v and (b) solar network k2v, (c) solar internetwork k2r (d) solar network k2r, (e) solar internetwork k3 and, (f) solar network k3.

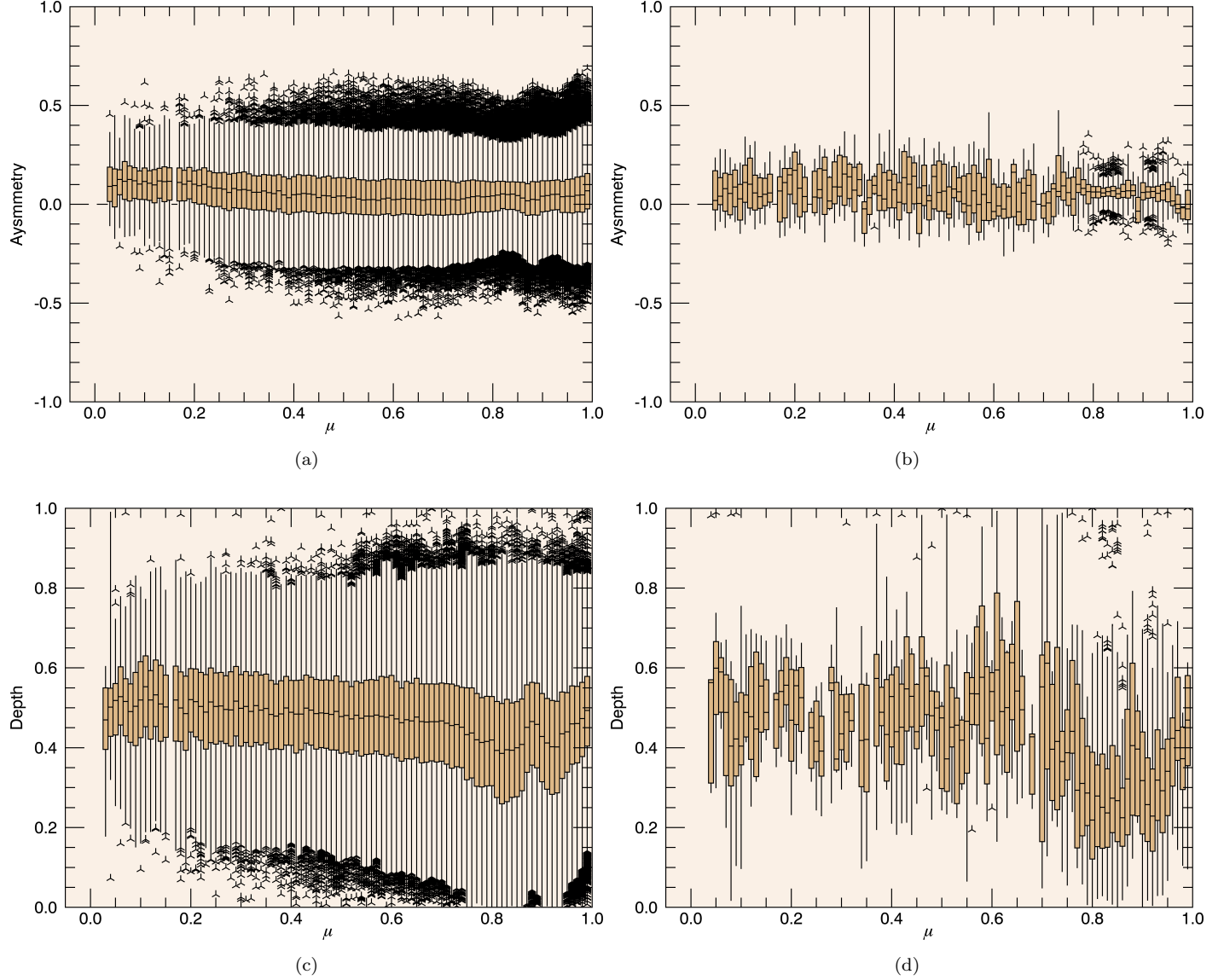


Figure 8. As figure 5. The centre-to-limb variation in (a) asymmetry in the solar internetwork, (b) asymmetry in the solar network, (c) central core relative depth in the solar internetwork, and (d) central core relative depth in the solar network.

any given value of μ one would expect that the inferred behaviour of the plasma from Mg II h agrees with that inferred from Mg II k.

Although some rely upon doppler shifting and wavelength measurements, which has not been investigated here, many of the developed diagnostic tools rely upon the intensity observed in the various features of the emission profiles for which a description of the spatial variation has been developed. In the internetwork it is consistently seen that the central depression increases in intensity up to $\mu \sim 0.9$, the intensity of this feature is understood to be anti-correlated to the height of the line formation. From this it is possible to deduce that moving from the limb to $\mu \sim 0.9$ the height at which line formation occurs, and thus the height at which the transition region is found, decreases i.e. it is found deeper in the atmosphere. Moving beyond $\mu \sim 0.9$ and closer to the disk centre, as the central depression intensity decreases this relationship implies that the height at which the transition region is found increases.

The intensities of the emission peaks reveal information about their temperature of formation, as this shows a strong correlation. In both Mg II h and Mg II k the maxima show an increase in intensity from the limb to $\mu \sim 0.9$, from this it can be deduced that the upper chromospheric plasma temperature increases from the limb towards the disk centre. This effect is, however, reversed moving closer to the disk centre as the intensities are seen to decrease resulting in a decrease in temperature.

There is a strong correlation between peak intensity and temperature of formation and a strong anti-correlation between the intensity of the central depression and the height of the transition region. As both of these intensities follow the same pattern of progression it is possible, therefore, to say that there is an anti-correlated relationship between the height of the transition region and the temperature of line formation.

It is also possible to determine the velocity seen in the upper chromosphere by studying the ratio of the intensities of the $*2v$ and $*2r$ peaks. Shown in figure 9 is the variation of the ratio of the intensity of the internetwork maxima in (a) Mg II h and (b) Mg II k over the solar disk. Although this shows a significant spread of values suggesting that there is a broad range of velocities present in the plasma of the upper chromosphere there does not appear to be a significant dependence on the location on the disk observed. This result is to be expected from the earlier figures presented as the asymmetry statistic is directly related to the ratio. From this it's easy to extend this analysis to the network. Although it is harder to see due to the aforementioned erraticism in

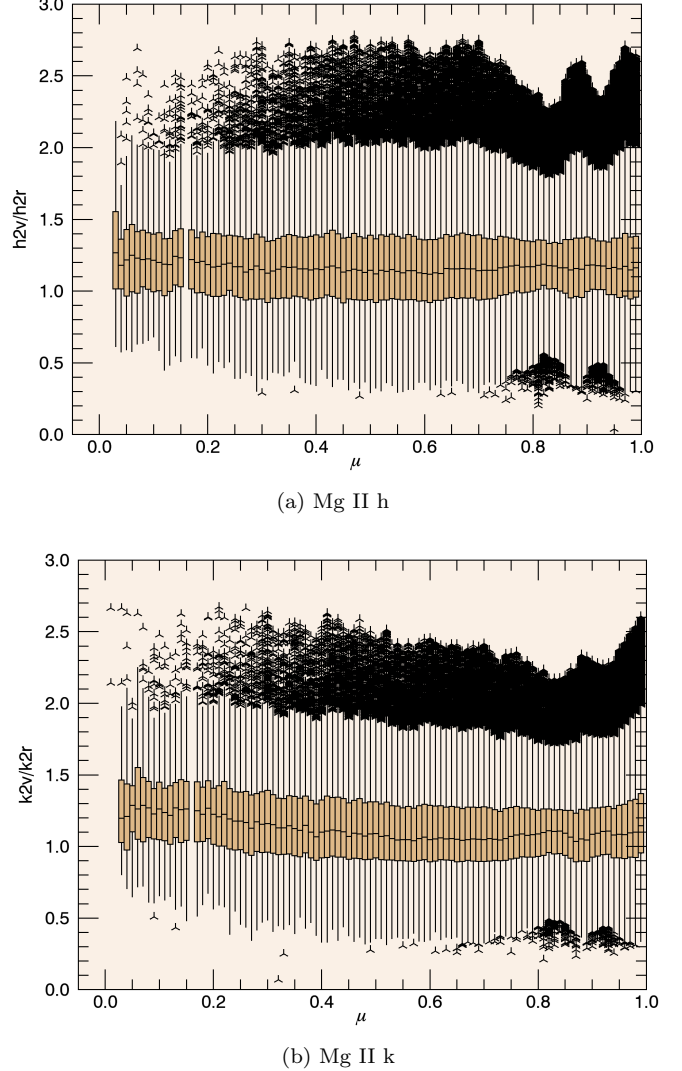


Figure 9. As figure 5. The centre to limb variation of the ratio of internetwork (a) $h2v$ and $h2r$, and (b) $k2v$ and $k2r$.

the spatial variation of the asymmetry statistic, it does follow a similar pattern to that seen in the internetwork with a broad spread of values but with no apparent dependency on disk location.

4.4. Temporal Variation of the Mg II Emission Lines

Since the start of the IRIS mission to the present day a full disk mosaic has been taken approximately once a month with the first mosaic taken on September 30th 2013 and the most recent on July 27th 2019 giving a total of 71 separate observations spanning approximately 6 years, which is just over half a solar cycle.

Shown in figure 10 is the variation of the $*2v$ and $*2r$ peaks in network Mg II h and Mg II k at different values of μ across the solar disk, namely at disk centre ($\mu = 1$) and at $\mu = 0.2$ at the limb. Although visible at

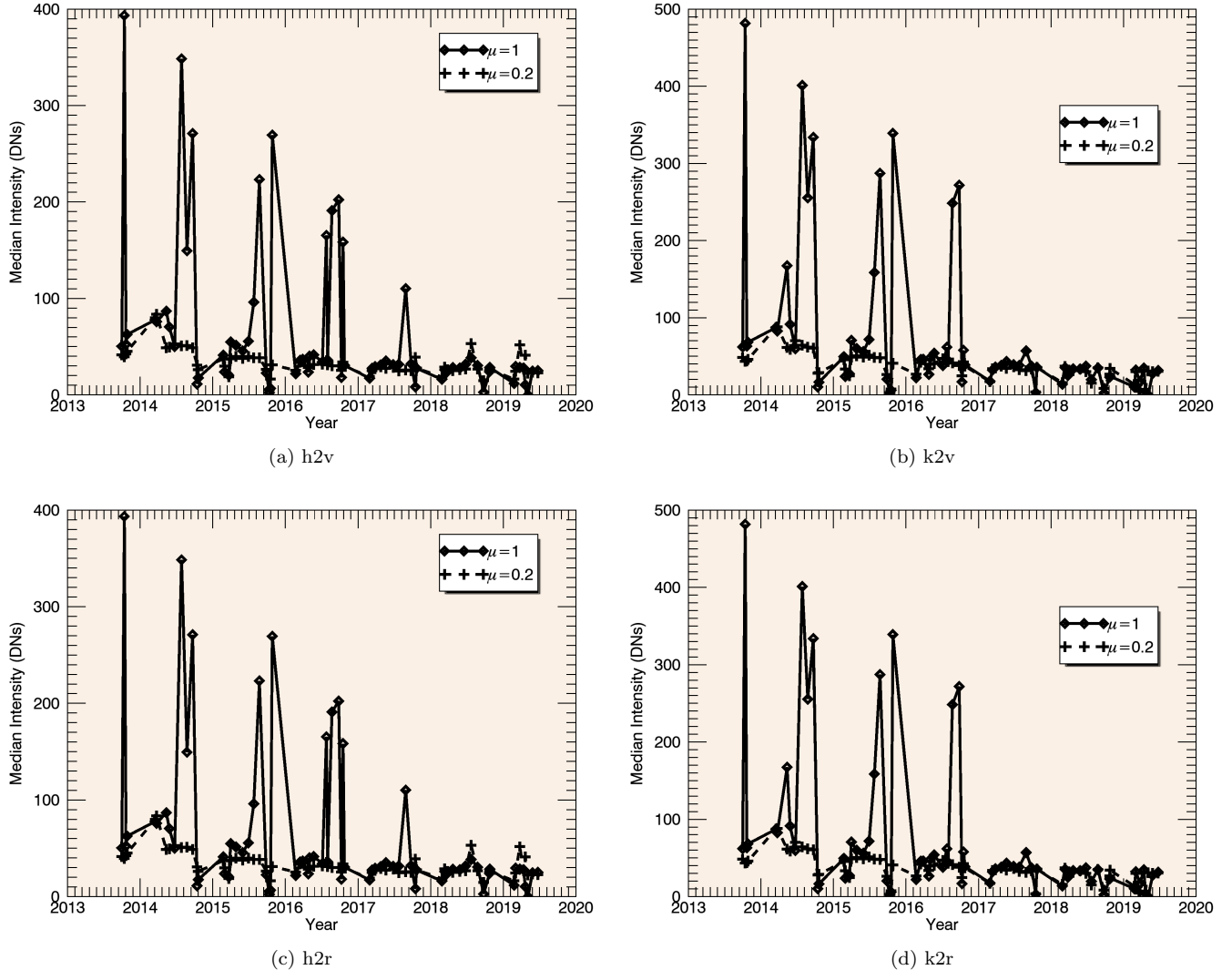


Figure 10. Variation in the median network intensity of (a) h2v in Mg II h, (b) k2v in Mg II k, (c) h2r in Mg II h, and (d) k2r in Mg II K across the duration of IRIS observations as observed at $\mu = 1$ and $\mu = 0.2$.

at both values of μ presented the temporal variation is far more obvious in the disk centre case, showing in all 4 studied features a marked decrease in median intensity from early time observations to present day. Although not included in the figures in order to preserve their clarity, investigation of the median observed intensity at a range of values of μ was carried out; in each case a similar trend could be visibility identified whereby the median intensity tends to decrease.

This trend of variation is as expected when considered with respect to the solar cycle. The period studied corresponds to the second half of solar cycle 24, which is understood to have started in December 2008 and is projected to come to an end in late 2019 (Meadows et al. 2019). As solar cycles run solar minimum to solar minimum, it would be expected that the observed intensities would demonstrate a sustained decreasing trend. Figure

11 shows the month on month variation in the 10.7 cm radio flux for the duration of the solar cycle, this can offer some comparison with the variation in the features seen in Mg II emission.

In both measures of the solar activity the observed intensity is seen to tend, from late 2013, to decrease towards 2019; this decrease though is not smooth in either Mg II or radio flux, but shows month to month spikes within this overall trend. Of interest within these spikes in intensity is the contemporaneous nature of their appearance in Mg II and radio. Comparison of these time series show that although the scale of these spikes does vary significantly, likely due to the difference in the emitting regions and processes seen in each method of observation, the link in presence appears throughout the period of study. The most directly comparable spikes in intensity that can be seen when looking at the me-

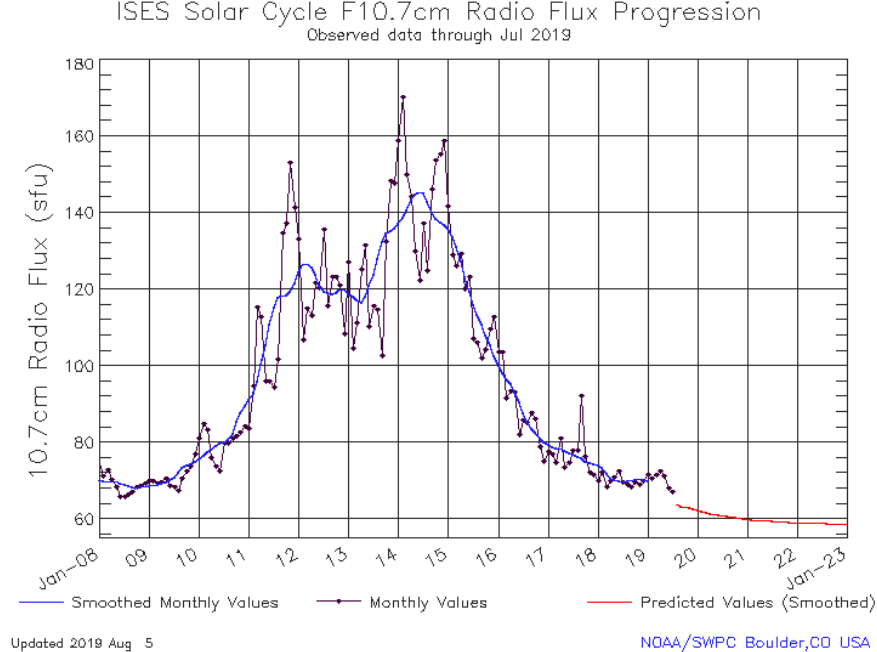


Figure 11. The 10.7cm radio flux from the sun as seen throughout solar cycle 24 (NOAA/SWPC 2019)

dian intensity at $\mu = 1$ in late 2017 in Mg II h there is a matching and strongly pronounced spike in intensity seen that this time in the radio flux, similarly an obvious matched spike can be seen in the median intensity at $\mu = 1$ in both Mg II h and Mg II k. In order to determine if there is any scientific merit to this observation it would be necessary to undertake further study directly comparing and analysing the underlying data. Furthermore it would be of interest to study the temporal variation of the median intensity of the emission features in the internetwork and identify if a similar relation to that previously described exists.

5. CONCLUSIONS

The launch of IRIS has provided unprecedented detail for the study of solar spectra, allowing us to see emission profiles that were previously hidden by the terrestrial atmosphere and in detail heretofore unavailable to us. Observations from IRIS have allowed for a plethora of difficulties inherent to solar astronomy to be overcome; such as only short periods of good seeing, allowing for long term observational stability that is not possible with ground based instruments.

The primary motivation for the study of spectral lines is to be able to make diagnosis of the physical properties and conditions of the solar atmosphere. These properties and conditions are linked to the nature of the spectral features observed and thus with the development of

suitable relations allow for direct inferences to be made about the nature of the solar atmosphere.

The purpose of this study was to build upon the methodology developed by Schmit et al. (2015) in order to study the spatial variation of the Mg II h emission line features; this methodology was taken further, noting the applicability of the model developed to study the spatial variation of the Mg II k emission line. It was necessary to take appropriate steps in the analysis to constrain the profile to avoid the unwanted effects of the nearby Mn I emission line. The results of the analysis of the Mg II h emission line features show good agreement with those found by Schmit et al. (2015) allowing for a high degree of confidence to be attributed to these findings. Based on this agreement and the very similar form of the Mg II k emission line profile the similar variation seen in this also allows for these results to also be considered a reliable description of the spatial variation.

The development of a description of the spatial variation in both of these emission lines allows for a description of the properties of the solar atmosphere to be developed. Using the model atmosphere and subsequent plasma diagnostics developed by Leenaarts et al. (2013a,b) and Pereira et al. (2013) it was possible to develop a description for the variation for many different properties of the solar atmosphere over the solar disk.

This study of the spatial variation of the emission lines and the plasma diagnostics has revealed that across the

disk there is significant variance in emission profiles and thus the atmospheric conditions. This variation shows that the height of the transition region varies significantly across the solar disk with a correlation to the manner in which the temperature varies across the disk. It was also seen that there was no dependence on disk location seen for the inferred line of sight velocity in the solar atmosphere.

The final part of this study was to look at how the spectral features of the emissions vary over the solar cycle. This study provided evidence of a link between the intensity of the emission features with the overall progression of the solar cycle and additionally provided evidence that short term increases in over all solar activity were also seen in the emission profiles. Better study of this possible link should be an avenue for future study,

potentially using cross-correlations to quantify any observed effect. It would further be instructive to extend the study of the temporal variation to the internetwork which was not investigated here.

I would like to thank Nicolas Labrosse for his support, guidance, and insight without which this work would not have been possible. I would also like to extend my gratitude to Norman Gray without whose knowledge and skill with a keyboard I would never have gotten so far.

IRIS is a NASA small explorer mission developed and operated by LMSAL with mission operations executed at NASA Ames Research centre and major contributions to downlink communications funded by ESA and the Norwegian Space Centre.

REFERENCES

- Carrington, R. C. 1858, MNRAS, 19, 1
- De Pontieu, B., Title, A. M., Lemen, J. R., et al. 2014, SoPh, 289, 2733
- Durand, E., Oberly, J. J., & Tousey, R. 1949, ApJ, 109, 1
- Gošić, M., Bellot Rubio, L. R., Orozco Suárez, D., Katsukawa, Y., & del Toro Iniesta, J. C. 2014, The Astrophysical Journal, 797, 49
- Hale, G. E. 1908, ApJ, 28, 315
- Hale, G. E., Ellerman, F., Nicholson, S. B., & Joy, A. H. 1919, ApJ, 49, 153
- Jørgensen, C. S., Karoff, C., Senthamizh Pavai, V., & Arlt, R. 2019, Solar Physics, 294, 77
- Kerr, G. S., Allred, J. C., & Carlsson, M. 2019, arXiv e-prints, arXiv:1908.05329
- Kohl, J. L., & Parkinson, W. H. 1976, ApJ, 205, 599
- Leenaarts, J., Pereira, T. M. D., Carlsson, M., Uitenbroek, H., & De Pontieu, B. 2013a, The Astrophysical Journal, 772, 89
- . 2013b, The Astrophysical Journal, 772, 90
- Markwardt, C. B. 2009, in Astronomical Society of the Pacific Conference Series, Vol. 411, Astronomical Data Analysis Software and Systems XVIII, ed. D. A. Bohlender, D. Durand, & P. Dowler, 251
- Meadows, P., Smith, L., & Cook, J. 2019, Journal of the British Astronomical Association, 129, 222
- Milkey, R. W., & Mihalas, D. 1974, ApJ, 192, 769
- NOAA/SWPC. 2019, Solar Cycle Progression, National Oceanic and Atmospheric Administration, provided as public domain from NOAA.SWPC
- Pereira, T. M. D., Leenaarts, J., De Pontieu, B., Carlsson, M., & Uitenbroek, H. 2013, The Astrophysical Journal, 778, 143
- Pereira, T. M. D., McIntosh, S. W., Pontieu, B. D., et al. 2019, A User's Guide to IRIS Data Retrieval, Reduction & Analysis, Tech. rep., IRIS
- Sánchez Almeida, J., & Martínez González, M. 2011, in Astronomical Society of the Pacific Conference Series, Vol. 437, Solar Polarization 6, ed. J. R. Kuhn, D. M. Harrington, H. Lin, S. V. Berdyugina, J. Trujillo-Bueno, S. L. Keil, & T. Rimmele, 451
- Scherrer, P. H., Schou, J., Bush, R. I., et al. 2012, SoPh, 275, 207
- Schmit, D., Bryans, P., Pontieu, B. D., et al. 2015, ApJ, 811, 127
- Schwabe, S. H. 1843, Astronomische Nachrichten, 20, 283
- Solanki, S. K. 1993, Space Science Reviews, 63, 1
- Spörer, G. 1880, Publikationen des Astrophysikalischen Observatoriums zu Potsdam, 5

APPENDIX

A. MASTER.PRO

```

1 arr_h= [2801.78:2805.28:0.035]
2 arr_k = [2794.65+(18*0.035):2798.15:0.035]
3 start_h = [4.41, 20.50, 2803.54, 575.76, 2803.53, 0.168, 0.93, 2803.53, 0.121]
4 start_k = [4.41, 20.50, 2796.4, 575.76, 2796.4, 0.168, 0.93, 2796.4, 0.121]
5
6 line = ''
7 read, line, prompt = 'MgIIf (h) or MgII (k): '
8
9 if line ne 'h' and line ne 'k' then begin
10   print, 'Try Again'
11   stop
12 endif
13
14 check = ''
15 read, check, prompt = 'Network(N) or Internetwork(I): '
16
17 if check ne 'N' and check ne 'I' then begin
18   print, 'Try Again'
19   stop
20 endif
21 files = file_search('Data '+line+/*MgII*.fits')
22
23 for n=0, size(files, /n_elements)-1, 1 do begin ;change starting value as needed
24   file='..'+files[n]
25   file_name = file_basename(file)
26
27 if strmatch(file_name, '*h*') then begin
28   cd, 'Results H'
29   Quiet_Sun, check, file, file_name, start_h, arr_h, line
30   Max_Min, check, file_name, arr_h
31 endif
32 if strmatch(file_name, '*k*') then begin
33   cd, 'Results K'
34   Quiet_Sun, check, file, file_name, start_k, arr_k, line
35   Max_Min, check, file_name, arr_k
36 endif
37
38 boxplotting, file_name, check
39 cd, '..'
40 endfor
41 end

```

B. QUIET_SUN.PRO

```

1 PRO Quiet_Sun, check, file, file_name, start, arr, line
2
3 if (ISA(shaped_dat_IRIS) eq 1) then begin
4   shaped_dat_IRIS = 0
5 endif
6
7 ;Reading in the data and modifying the fits files so they are readable later on
8 dat_IRIS = readfits(file, hdr)
9 sxdelpar, hdr, ['CTYPE1', 'CTYPE2', 'CTYPE3', 'CDELT3', 'CRPIX3', 'CRVAL3', 'CUNIT3', 'NAXIS3']

```

```

10 sxaddpar, hdr, 'NAXIS', '2'
11
12 dat_HMI = readfits('..../Data '+line+ '/'+strmid(file_name, 11, 8) + '_HMI.fits', hdu)
13 dat_HMI = abs(dat_HMI)
14
15 ;reshaping the data and the fits files
16 hcongrid, dat_HMI, hdu, shaped_dat_HMI, new_hdu, 1002, 4096
17
18 hcongrid, hdr
19
20 ;finding the solar x and y coordinates
21 new_header_IRIS = fitshead2struct(hdr)
22 new_wcs_IRIS = fitshead2wcs(new_header_IRIS)
23 coord_IRIS = wcs_get_coord(new_wcs_IRIS)
24
25 new_header_HMI = fitshead2struct(new_hdu)
26 new_wcs_HMI = fitshead2wcs(new_header_HMI)
27 coord_HMI = wcs_get_coord(new_wcs_HMI)
28
29 ;finding the size of the sun in the image
30 slice_HMI = shaped_dat_HMI[501,*]
31 radius_HMI = (size(where(slice_HMI gt 0.), /n_elements))/2
32
33 ;finding the locations in HMI of quiet sun
34
35 if check eq 'N' then begin
36   ind = WHERE_XYZ(shaped_dat_HMI gt 60. and shaped_dat_HMI lt 200., XIND=xind, YIND=yind)
37 endif
38 if check eq 'I' then begin
39   ind = WHERE_XYZ(shaped_dat_HMI gt 0. and shaped_dat_HMI lt 60., XIND=xind, YIND=yind)
40 endif
41
42 IRIS_quiet_coord=[0,0]
43
44 shaped_dat_IRIS = congrid(dat_IRIS, 1002, 4096, 101)
45 slice_IRIS = shaped_dat_IRIS[501,*,50]
46 radius_IRIS = (size(where(slice_IRIS gt 0.), /n_elements))/2
47
48 ;calculating full set of results
49 results=[0]
50 chi_sqr=[0]
51 iteration_num=[0]
52 for y=0, size(XIND, /n_elements)-1 do begin
53
54   count = 0
55   ;use the fits header to establish what the limits here should be
56   for s=-5, 5 do begin
57     for t=-5,5 do begin
58       true_dist = sqrt(s^2+t^2)
59       if true_dist gt 5. then continue
60       if check eq 'N' then begin
61         if shaped_dat_HMI[(xind[y]+s), (yind[y]+t)] gt 60. and shaped_dat_HMI[(xind[y]+s), (yind[y]+t)]
62           lt 200. then count++
63       endif
64       if check eq 'I' then begin
65         if shaped_dat_HMI[(xind[y]+s), (yind[y]+t)] gt 0. and shaped_dat_HMI[(xind[y]+s), (yind[y]+t)]
66           lt 60. then count++
67       endif
68     endfor

```

```

67      endfor
68
69      if check eq 'N' and count lt 23 then continue
70      if check eq 'I' and count gt 147 then continue
71
72      iteration_num = append(iteration_num, y)
73
74      IRIS_quiet_coord = append(IRIS_quiet_coord, [nearest_index(coord_HMI[0,xind[y]], coord_IRIS[0,*]),
75                                     nearest_index(coord_HMI[1,0,yind[y]], coord_IRIS[1,0,*])])
76
77      result = MPFITFUN('model', arr, shaped_dat_IRIS[nearest_index(coord_HMI[0, xind[y]], coord_IRIS[0,*]),
78                               nearest_index(coord_HMI[1,0, yind[y]], coord_IRIS[1,0,*]), 101-size(arr, /n_elements):*],
79                               sqrt(shaped_dat_IRIS[nearest_index(coord_HMI[0, xind[y]], coord_IRIS[0,*]),
80                                     nearest_index(coord_HMI[1,0, yind[y]], coord_IRIS[1,0,*]), 101-size(arr, /n_elements):*]), start,
81                               /quiet)
82
83      if (size(result, /n_elements) eq 10) then begin
84          if (finite(result[9])) eq 1 then begin
85              results = append(results, result[0:8])
86              chi_sqr = append(chi_sqr, result[9])
87          endif else begin
88              results = append(results, [!values.f_nan])
89              chi_sqr = append(chi_sqr, result[9])
90          endelse
91      endif else begin
92          if (size(result, /n_elements) eq 2) then begin
93              results = append(results, result[0])
94              chi_sqr = append(chi_sqr, result[1])
95          endif else begin
96              results = append(results, result[0])
97              chi_sqr = append(chi_sqr, result[0])
98          endelse
99      endelse
100  endfor
101
102  shaped_dat_iris = 0
103
104  mu = cos(asin(sqrt((coord_IRIS[0,501,0]-IRIS_quiet_coord[0::2])^2+(coord_IRIS[1,0,2048] -
105      IRIS_quiet_coord[1::2])^2)/(radius_IRIS*(fxpar(hdr, 'CDELT1')))))
106  mu = [[0], mu]
107  total_iteration = size(iteration_num, /n_elements)
108  results_nan = [[0],where(~finite(results), /null)]
109  chi_sqr_nan = [[0], where(~finite(chi_sqr), /null)]
110
111  ;construct a new n by 2 array containing the x and y pairs
112
113  IRIS_quiet_coord_x = IRIS_quiet_coord[0::2]
114  IRIS_quiet_coord_y = IRIS_quiet_coord[1::2]
115
116  ;remove the results that could not be fitted
117  if size(results_nan, /n_elements) eq size(results, /n_elements) then return
118  remove, results_nan, results
119  remove, chi_sqr_nan, mu
120  remove, chi_sqr_nan, chi_sqr
121  remove, chi_sqr_nan, IRIS_quiet_coord_x, IRIS_quiet_coord_y
122  remove, chi_sqr_nan, iteration_num
123
124  IRIS_quiet_coord_xy = fltarr(2, size(IRIS_quiet_coord_x, /n_elements))
125  IRIS_quiet_coord_xy[0,*] = IRIS_quiet_coord_x

```

```

120  IRIS_quiet_coord_xy[1,*] = IRIS_quiet_coord_y
121
122 ;remove the 'bad' fits
123 bad_fit = where((chi_sqr/size(arr, /n_elements)) gt 1.5)
124 remove, bad_fit, mu
125 acceptance_ratio = (float(size(mu, /n_elements))/float(total_iteration))*100.
126 a=long64(0)
127 for n = 0, size(results, /n_elements)-8, 9 do begin
128   locs = where(n eq bad_fit*9)
129   if locs[0] ne -1 then continue
130   ++a
131   modeled = model(arr, results[n:n+8])
132   if check eq 'I' then begin
133     file_mkdir, 'modelled_internetwork_' + strmid(file_name,11,8)
134     openw, 1, './modelled_internetwork_' + strmid(file_name,11,8) + '/modelled_' + string(a) + '.txt',
135       width=4000
136     endif
137   if check eq 'N' then begin
138     file_mkdir, 'modelled_network_' + strmid(file_name,11,8)
139     openw, 1, './modelled_network_' + strmid(file_name, 11, 8) + '/modelled_' + string(a) + '.txt',
140       width=4000
141     endif
142     printf, 1, modeled
143     close, 1
144   endfor
145   mu_arr = make_array(1, size(mu, /n_elements), /float, value=1.1)
146   mu_arr[0,*] = mu
147
148   openw, 2, 'fits.txt'
149   printf, 2, results
150   close, 2
151
152   if check eq 'I' then begin
153     if file_test('mu_internetwork') eq 0 then begin
154       file_mkdir, 'mu_internetwork'
155     endif
156     openw, 3, './mu_internetwork/mu_' + strmid(file_name, 11, 8) + '.txt'
157     printf, 3, mu_arr
158     close, 3
159   endif
160   if check eq 'N' then begin
161     if file_test('mu_network') eq 0 then begin
162       file_mkdir, 'mu_network'
163     endif
164     openw, 3, './mu_network/mu_' + strmid(file_name, 11, 8) + '.txt'
165     printf, 3, mu_arr
166     close, 3
167   endif
168
169   print, 'Acceptance Percentage = '
170   print, acceptance_ratio

```

C. MAX_MIN.PRO

```

1 PRO Max_Min, check, file_name, arr
2
3

```

```

4 if check eq 'N' then begin
5 if file_test('modelled_network_'+strmid(file_name, 11, 8)) eq 0 then return
6 cd, 'mu_network'
7 data = read_ascii('mu_'+strmid(file_name, 11, 8)+'.txt')
8 cd, '../modelled_network_ '+strmid(file_name, 11, 8)
9 endif
10 if check eq 'I' then begin
11 if file_test('modelled_internetwork_'+strmid(file_name, 11, 8)) eq 0 then return
12 cd, 'mu_internetwork'
13 data = read_ascii('mu_'+strmid(file_name, 11, 8)+'.txt')
14 cd, '../modelled_internetwork_ '+strmid(file_name, 11, 8)
15 endif
16 mu = data.(0)
17 mu = reshape(mu, fltarr(size(mu, /n_elements)))
18
19 max_values = fltarr(2,size(mu, /n_elements))
20 min_values = fltarr(3,size(mu, /n_elements))
21 for n = 1, size(mu, /n_elements)-1 do begin
22   data = read_ascii('modelled_ ' + string(long64(n)) + '.txt')
23   maxes = data.(0)[local_max_finder(arr, data.(0))]
24   if (size(maxes, /n_elements) gt 4) then begin
25     loc = where(maxes eq min(maxes))
26     remove, loc, maxes
27     endif
28   if (size(maxes, /n_elements) gt 3) then begin
29     loc = where(maxes eq min(maxes))
30     remove, loc, maxes
31     endif
32   if (size(maxes, /n_elements) gt 2) then begin
33     loc = where(maxes eq min(maxes))
34     remove, loc, maxes
35     endif
36   if (size(maxes, /n_elements) lt 1) then begin
37     maxes = [maxes, [|values.F_nan|]]
38     endif
39   if (size(maxes, /n_elements) lt 2) then begin
40     maxes = [maxes, [|values.F_NAN|]]
41     endif
42   max_values[*,n-1] = maxes
43
44 mins = data.(0)[local_max_finder(arr, data.(0), /minima)]
45   if (size(mins, /n_elements) lt 1) then begin
46     mins = [mins, [|values.F_NAN|]]
47     endif
48   if (size(mins, /n_elements) lt 2) then begin
49     mins = [mins, [|values.F_NAN|]]
50     endif
51   if (size(mins, /n_elements) lt 3) then begin
52     mins = [mins, [|values.F_NAN|]]
53     endif
54   if (size(mins, /n_elements) gt 5) then begin
55     loc = where(mins eq max(mins))
56     remove, loc, mins
57     endif
58   if (size(mins, /n_elements) gt 4) then begin
59     loc = where(mins eq max(mins))
60     remove, loc, mins
61     endif
62   if (size(mins, /n_elements) gt 3) then begin

```

```

63 loc = where(mins eq max(mins))
64 remove, loc, mins
65 endif
66 min_values[*,n-1] = mins
67 endfor
68 cd, '../'
69
70 if check eq 'I' then begin
71   if file_test('internetwork_maxes') eq 0 then begin
72     file_mkdir, 'internetwork_maxes'
73   endif
74   if file_test('internetwork_mins') eq 0 then begin
75     file_mkdir, 'internetwork_mins'
76   endif
77   openw, 1, 'internetwork_maxes/maxes_values_'+strmid(file_name, 11, 8)+'.txt'
78   printf, 1, max_values
79   close, 1
80   openw, 2, 'internetwork_mins/mins_values_'+strmid(file_name, 11, 8)+'.txt'
81   printf, 2, min_values
82   close, 2
83 endif
84 if check eq 'N' then begin
85   if file_test('network_maxes') eq 0 then begin
86     file_mkdir, 'network_maxes'
87   endif
88   if file_test('network_mins') eq 0 then begin
89     file_mkdir, 'network_mins'
90   endif
91   openw, 1, 'network_maxes/maxes_values_'+strmid(file_name, 11, 8)+'.txt'
92   printf, 1, max_values
93   close, 1
94   openw, 2, 'network_mins/mins_values_'+strmid(file_name, 11, 8)+'.txt'
95   printf, 2, min_values
96   close, 2
97 endif
98
99 end

```

D. BOXPLOTTING.PRO

```

1 PRO boxplotting, file_name, check
2
3
4 if check eq 'N' then begin
5 if file_test('modelled_network_'+strmid(file_name, 11, 8)) eq 0 then return
6 cd, 'mu_network'
7 data = read_ascii('mu_'+strmid(file_name, 11, 8)+'.txt')
8 cd, '../network_maxes'
9 data_1 = read_ascii('maxes_values_'+strmid(file_name, 11, 8)+'.txt')
10 cd, '../network_mins'
11 data_2 = read_ascii('mins_values_'+strmid(file_name, 11, 8)+'.txt')
12 cd, '../'
13 endif
14 if check eq 'I' then begin
15 if file_test('modelled_internetwork_'+strmid(file_name, 11, 8)) eq 0 then return
16 cd, 'mu_internetwork'
17 data = read_ascii('mu_'+strmid(file_name, 11, 8)+'.txt')
18 cd, '../internetwork_maxes'
19 data_1 = read_ascii('maxes_values_'+strmid(file_name, 11, 8)+'.txt')

```

```

20 cd, '../internetwork_mins'
21 data_2 = read_ascii('mins_values_'+strmid(file_name, 11, 8)+'.txt')
22 cd, '../'
23 endif
24 mu = data.(0)
25 mu = reshape(mu, fltarr(size(mu, /n_elements)))
26 max_values = data_1.(0)
27 min_values = data_2.(0)
28
29 goodval = where(Finite(mu), /null)
30 rounded =(Round(mu[goodval]*100.)/100.)
31 peak1 = max_values[0, goodval]
32 peak2 = max_values[1, goodval]
33 minima = min_values[1, goodval]
34
35 asym = (max_values[0,goodval]-max_values[1,goodval])/(max_values[0,goodval]+max_values[1,goodval])
36 depth = 1. - ((2.*min_values[1,goodval])/(max_values[0,goodval]+max_values[1,goodval]))
37
38 i= [0.01:0.99:0.01]
39
40 boxes_1 = fltarr(99,5)
41 boxes_2 = fltarr(99,5)
42 boxes_3 = fltarr(99,5)
43 boxes_4 = fltarr(99,5)
44 boxes_5 = fltarr(99,5)
45
46 for l = 0.02, 0.99, 0.01 do begin
47   if size(where(rounded eq round(l*100)/100., /null), /n_elements) lt 5 then continue
48   if size(where(finite(peak1[0, where(rounded eq round(l*100)/100., /null)]), /n_elements) lt 5 then
49     goto, JUMP1
50   boxes_1[fix(l*100.),*] = createboxplotdata(peak1[0, where(rounded eq round(l*100)/100., /null)],
51     suspected_outlier_values=a)
52
53   if array_equal(boxes_1[fix(l*100.), *], (boxes_1[fix(l*100.), *])[sort(boxes_1[fix(l*100.), *])]) eq 0 then
54     boxes_1[fix(l*100.), *] = [0,0,0,0,0]
55
56   if isa(a) eq 1 then begin
57     a[0,*] = fix(l*100.)
58   endif
59   if isa(outliers_1) eq 0 then begin
60     outliers_1 = a
61   endif else begin
62     outliers_1 = [[outliers_1],[a]]
63   endelse
64
65   JUMP1:if size(where(finite(peak2[0, where(rounded eq round(l*100)/100., /null)]), /n_elements) lt 5
66     then goto, JUMP2
67   boxes_2[fix(l*100.),*] = createboxplotdata(peak2[0, where(rounded eq round(l*100)/100., /null)],
68     suspected_outlier_values=b)
69
70   if array_equal(boxes_2[fix(l*100.), *], (boxes_2[fix(l*100.), *])[sort(boxes_2[fix(l*100.), *])]) eq 0 then
71     boxes_2[fix(l*100.), *] = [0,0,0,0,0]
72
73   if isa(b) eq 1 then begin
74     b[0,*] = fix(l*100.)
75   endif
76   if isa(outliers_2) eq 0 then begin
77     outliers_2 = b
78   endif else begin

```

```

73 outliers_2 = [[outliers_2], [b]]
74 endelse
75
76 JUMP2:if size(where(finite(minima[0, where(rounded eq round(l*100)/100., /null)]), /null), /n_elements) lt
    5 then goto, JUMP3
77 boxes_3[fix(l*100.)*] = createboxplotdata(minima[0, where(rounded eq round(l*100)/100., /null)],
    suspected_outlier_values=c)
78
79 if array_equal(boxes_3[fix(l*100.), *], (boxes_3[fix(l*100.), *])[sort(boxes_3[fix(l*100.), *])]) eq 0 then
    boxes_3[fix(l*100.), *] = [0,0,0,0,0]
80
81 if isa(c) eq 1 then begin
82 c[0, *] = fix(l*100.)
83 endif
84 if isa(outlier_3) eq 0 then begin
85 outliers_3 = c
86 endif else begin
87 outliers_3 = [[outliers_3], [c]]
88 endelse
89
90 JUMP3:if size(where(finite(asym[0, where(rounded eq round(l*100)/100., /null)]), /null), /n_elements) lt 5
    then goto, JUMP4
91 boxes_4[fix(l*100.)*] = createboxplotdata(asym[0, where(rounded eq round(l*100)/100., /null)],
    suspected_outlier_values=d)
92
93 if array_equal(boxes_4[fix(l*100.), *], (boxes_4[fix(l*100.), *])[sort(boxes_4[fix(l*100.), *])]) eq 0 then
    boxes_4[fix(l*100.), *] = [0,0,0,0,0]
94
95 if isa(d) eq 1 then begin
96 d[0,*] = fix(l*100.)
97 endif
98 if isa(outliers_4) eq 0 then begin
99 outliers_4 = d
100 endif else begin
101 outliers_4 = [[outliers_4], [d]]
102 endelse
103
104 JUMP4:if size(where(finite(depth[0, where(rounded eq round(l*100)/100., /null)]), /null), /n_elements) lt 5
    then continue
105 boxes_5[fix(l*100.)*] = createboxplotdata(depth[0, where(rounded eq round(l*100)/100., /null)],
    suspected_outlier_values=e)
106
107 if array_equal(boxes_5[fix(l*100.), *], (boxes_5[fix(l*100.), *])[sort(boxes_5[fix(l*100.), *])]) eq 0 then
    boxes_5[fix(l*100.), *] = [0,0,0,0,0]
108
109 if isa(e) eq 1 then begin
110 e[0,*] = fix(l*100.)
111 endif
112 if isa(outliers_5) eq 0 then begin
113 outliers_5 = e
114 endif else begin
115 outliers_5 = [[outliers_5], [e]]
116 endelse
117
118 endfor
119
120 z = boxplot(i, boxes_1, suspected_outlier_values=outliers_1, width=0.005, xrange=[-0.05,1], yrange = [0,
    round(max(bboxes_1)/100.)*100], FILL_COLOR='burlywood', BACKGROUND_COLOR='linen', endcaps=0)
121 z.symbol_suspected_outliers.symbol=13

```

```

122 z.ytitle='Peak Intensity (DNs)'
123 z.xtitle='$\mu$'
124 z.title='h2v'
125
126 y = boxplot(i,boxes_2,suspected_outlier_values=outliers_2, width=0.005, xrange=[-0.05,1],yrange = [0,
127     round(max(boxes_2)/100.)*100],FILL_COLOR='burlywood', BACKGROUND_COLOR='linen', endcaps=0)
128 y.symbol_suspected_outliers.symbol=13
129 y.ytitle='Peak Intensity (DNs)'
130 y.xtitle='$\mu$'
131 y.title='h2r'
132
133 x = boxplot(i,boxes_3,suspected_outlier_values=outliers_3, width=0.005, xrange=[-0.05,1],yrange = [0,
134     round(max(boxes_3)/100.)*100],FILL_COLOR='burlywood', BACKGROUND_COLOR='linen', endcaps=0)
135 x.symbol_suspected_outliers.symbol=13
136 x.ytitle='Peak Intensity (DNs)'
137 x.xtitle='$\mu$'
138 x.title='h3'
139
140 t = boxplot(i,boxes_4,suspected_outlier_values=outliers_4, width=0.005, xrange=[-0.05,1],yrange = [-1,
141     1],FILL_COLOR='burlywood', BACKGROUND_COLOR='linen', endcaps=0)
142 t.symbol_suspected_outliers.symbol=13
143 t.ytitle='Aysmmetry'
144 t.xtitle='$\mu$'
145
146 s = boxplot(i,boxes_5,suspected_outlier_values=outliers_5, width=0.005, xrange=[-0.05,1],yrange = [0,
147     1],FILL_COLOR='burlywood', BACKGROUND_COLOR='linen', endcaps=0)
148 s.symbol_suspected_outliers.symbol=13
149 s.ytitle='Depth'
150 s.xtitle='$\mu$'
151
152 if check eq 'N' then begin
153   if file_test('network_boxes') eq 0 then begin
154     file_mkdir, 'network_boxes'
155   endif
156   cd, 'network_boxes'
157   z.save, 'h2v_box_'+ strmid(file_name, 11, 8)+'.png', border=10, resoultion=300
158   y.save, 'h2r_box_'+strmid(file_name, 11, 8)+'.png', border=10, resoultion=300
159   x.save, 'h3_box_'+ strmid(file_name, 11, 8)+'.png', border=10, resoultion=300
160   s.save, 'depth_'+ strmid(file_name, 11, 8)+'.png', border=10, resoultion=300
161   t.save, 'aysmmetry_'+ strmid(file_name, 11, 8)+'.png', border=10, resoultion=300
162   endif
163   if check eq 'I' then begin
164     if file_test('internetwork_boxes') eq 0 then begin
165       file_mkdir, 'internetwork_boxes'
166     endif
167     cd, 'internetwork_boxes'
168     z.save, 'h2v_box_'+ strmid(file_name, 11, 8)+'.png', border=10, resoultion=300
169     y.save, 'h2r_box_'+strmid(file_name, 11, 8)+'.png', border=10, resoultion=300
170     x.save, 'h3_box_'+ strmid(file_name, 11, 8)+'.png', border=10, resoultion=300
171     s.save, 'depth_'+ strmid(file_name, 11, 8)+'.png', border=10, resoultion=300
172     t.save, 'aysmmetry_'+ strmid(file_name, 11, 8)+'.png', border=10, resoultion=300
173   endif
174   z.close
175   y.close
176   x.close
177   s.close
178   t.close

```

```

177
178 | cd, '.../`'
179 |
180 | end

```

E. RATIOS.PRO

```

1 data = read_ascii('Results H/internetwork_maxes/maxes_values_20140824.txt')
2 h_maxes = data.(0)
3 data = read_ascii('Results K/internetwork_maxes/maxes_values_20140824.txt')
4 k_maxes = data.(0)
5 data = read_ascii('Results H/mu_internetwork/mu_20140824.txt')
6 h_mu = data.(0)
7 data = read_ascii('Results K/mu_internetwork/mu_20140824.txt')
8 k_mu = data.(0)
9
10 h_ratio = h_maxes[0,*]/h_maxes[1,*]
11 k_ratio = k_maxes[0,*]/k_maxes[1,*]
12
13 h_mu_badval = where(~finite(h_mu), /null)
14 k_mu_badval = where(~finite(k_mu), /null)
15
16 remove, h_mu_badval, h_mu, h_ratio
17 remove, k_mu_badval, k_mu, k_ratio
18
19 h_ratio_badval = where(~finite(h_ratio), /null)
20 k_ratio_badval = where(~finite(k_ratio), /null)
21
22 remove, h_ratio_badval, h_mu, h_ratio
23 remove, k_ratio_badval, k_mu, k_ratio
24
25 rounded_h = (round(h_mu*100.)/100.)
26 rounded_k = (round(k_mu*100.)/100.)
27
28 boxes_1 = fltarr(99, 5)
29 boxes_2 = fltarr(99, 5)
30 i = [0.01:0.99:0.01]
31
32 for l = 0.02, 0.99, 0.01 do begin
33 boxes_1[fix(l*100.),*] = createboxplotdata(h_ratio[where(rounded_h eq round(l*100)/100., /null)],
34   suspected_outlier_values=a)
35 boxes_2[fix(l*100.),*] = createboxplotdata(k_ratio[where(rounded_k eq round(l*100)/100., /null)],
36   suspected_outlier_values=b)
37
38 if isa(a) eq 1 then begin
39   a[0,*] = fix(l*100.)
40 endif
41 if isa(outliers_1) eq 0 then begin
42   outliers_1 = a
43 endif else begin
44   outliers_1 = [[outliers_1],[a]]
45 endif
46
47 if isa(b) eq 1 then begin
48   b[0,*] = fix(l*100.)
49 endif
50 if isa(outliers_2) eq 0 then begin
51   outliers_2 = b
52 endif else begin

```

```

51 outliers_2 = [[outliers_2],[b]]
52 endelse
53 endfor
54
55 t = boxplot(i, boxes_1, suspected_outlier_values=outliers_1, width = 0.005, xrange=[-0.05, 1],
56   FILL_COLOR='burlywood', background_color='linen', endcaps=0)
57 t.symbol_suspected_outliers.symbol=13
58 t.xtitle='$\mu$'
59 t.ytitle='h2v/h2r'
60
61 s = boxplot(i, boxes_2, suspected_outlier_values=outliers_2, width = 0.005, xrange=[-0.05, 1],
62   FILL_COLOR='burlywood', background_color='linen', endcaps=0)
63 s.symbol_suspected_outliers.symbol=13
64 s.xtitle='$\mu$'
65 s.ytitle='k2v/k2r'
66
67 t.save, 'h_peak_ratio.png', border=10, resolution=300
68 s.save, 'k_peak_ratio.png', border=10, resolution=300
69
70 end

```

F. TEMPORAL.PRO

```

1 line = ''
2 read, line, prompt = 'MgIIh (H) or MgII (K): '
3
4 if line ne 'H' and line ne 'K' then begin
5   print, 'Try Again'
6   stop
7 endif
8
9 check = ''
10 read, check, prompt = 'Network(N) or Internetwork(I): '
11
12 if check ne 'N' and check ne 'I' then begin
13   print, 'Try Again'
14   stop
15 endif
16 cd, 'Results '+line
17 if check eq 'N' then begin
18   files_max = file_search('network_maxes/*.txt')
19   files_mu = file_search('mu_network/*.txt')
20 endif
21 if check eq 'I' then begin
22   files_max = file_search('internetwork_maxes/*.txt')
23   files_mu = file_search('mu_internetwork/*.txt')
24 endif
25
26 files_fits = file_search('../Data h/*_HMI.fits')
27
28 dates = fltarr(1, size(files_max, /n_elements))
29 median_02 = fltarr(2, size(files_max, /n_elements))
30 median_04 = fltarr(2, size(files_max, /n_elements))
31 median_06 = fltarr(2, size(files_max, /n_elements))
32 median_08 = fltarr(2, size(files_max, /n_elements))
33 median_1 = fltarr(2, size(files_max, /n_elements))
34
35 for n=0, size(files_max, /n_elements)-1 do begin

```

```

37 data = readfits(files_fits[n], hdu)
38
39 dates[0, n] = date_conv(sxpar(hdu, 'DATE_OBS'), 'J')
40
41 file_max = files_max[n]
42 file_mu = files_mu[n]
43
44 mu_data = read_ascii(file_mu)
45 mu = mu_data.(0)
46 mu = (round(mu*10.)/10.)
47
48 max_data = read_ascii(file_max)
49 max_values = max_data.(0)
50
51 locs = where(mu eq 0.2)
52 max_02 = max_values[*,locs]
53 median_02[*, n] = median(max_02)
54
55 locs = where(mu eq 0.4)
56 max_04 = max_values[*,locs]
57 median_04[*, n] = median(max_04)
58
59 locs = where(mu eq 0.6)
60 max_06 = max_values[*,locs]
61 median_06[*, n] = median(max_06)
62
63 locs = where(mu eq 0.8)
64 max_08 = max_values[*,locs]
65 median_08[*, n] = median(max_08)
66
67 locs = where(mu eq 1.)
68 max_1 = max_values[*,locs]
69 median_1[*, n] = median(max_1)
70 endfor
71 cd, '../'
72 z = plot(dates, median_1[1, *], xtickunits='years', linestyle = 0, symbol = 'D', name = '$\mu=1$', background_color = 'linen', thick = 3, sym_thick=3, ytitle='Median Intensity (DNs)', xtitle='Year')
73 ;z1 = plot(dates, median_04[0, *], /overplot, linestyle = 1, symbol = 'tu', name = '$\mu=0.6$')
74 ;z2 = plot(dates, median_06[0, *], /overplot, linestyle = 2, symbol = '*', name = '$\mu=0.5$')
75 ;z3 = plot(dates, median_08[0, *], /overplot, linestyle = 3, symbol = 's', name = '$\mu=0.4$')
76 z4 = plot(dates, median_02[1, *], /overplot, linestyle = 2, symbol = '+', name = '$\mu=0.2$', sym_thick=3, thick=3)
77 leg = legend(target=[z, z4], position = [dates[n-1], 375], /data, /auto_text_color, /device)
78
79 z.save, line+check+_temporal_r.png, border=10, resolution=300
80 end

```